Yang *et al. Geothermal Energy* (2024) 12:3
https://doi.org/10.1186/s40517-024-00282-w

Geothermal Energy

RESEARCH Open Access

Calculation model and influence factors of thermal conductivity of composite cement-based materials for geothermal well

Yu Yang[1,2], Bo Li[1,2*], Lulu Che[1,2], Menghua Li[1,2], Ye Luo[1,2,3] and Hang Han[1]

*Correspondence: libo1512@163.com

[1] Key Laboratory of Karst Georesources and Environment, Ministry of Education, Guizhou University, Guiyang 550025, China
[2] College of Resource and Environmental Engineering, Guizhou University, Guiyang 550025, China
[3] Guizhou Kailin (Group) Co., Ltd, Guiyang 550000, China

Abstract

The use of cement-based composites (CBC) with high thermal conductivity for geothermal well cementing is extremely important for the efficient development and use of geothermal energy. Accurate prediction of thermal conductivity can save a lot of experimental costs and time. At present, there is no specific calculation model for the thermal conductivity of CBC. In this study, the microstructure, thermal conductivity model and influencing factors of CBC were investigated by experimental tests, theoretical analysis and numerical simulation. The results showed that the cement-based material could be simplified into a two-layer structure of hydrated and unhydrated layers. Mathematical and numerical models based on the coupled Series model and the Maxwell–Eucken model were established to calculate the thermal conductivity for CBC. The mathematical and numerical models were found to be more accurate by comparison with the conventional models and experimental test results. The cubic packing was more favorable than the spherical packing to improve the thermal conductivity of CBC. The plate material had significant anisotropy. The thermal conductivity of CBC showed a rapid decrease followed by a slow decrease, a decrease followed by a slow increase and finally a rapid decrease, a rapid increase followed by an up and down fluctuation and finally a plateau, respectively, with the increase of filler particle diameter, spacing and curing temperature. Based on these results, the effective methods and future research directions were proposed to maximize the thermal conductivity of geothermal well cementing materials in actual engineering applications. The research findings can provide some technical references for the efficient development of geothermal energy and research on CBC with high thermal conductivity.

Keywords: Geothermal energy, Cement-based composite, Microstructure, Thermal conductivity model, Thermal conductivity filler, Numerical simulation

Introduction

The massive exploitation and overuse of primary fossil energy sources has caused a serious environmental crisis and energy shortage, which has gradually become a central issue of concern for countries around the world. The search for alternative clean energy sources has become a very urgent solution (Carvajal et al. 2022; Rajvikram et al. 2022). Various energy sources such as solar, wind, hydro, and biomass have been widely

developed. However, they are heavily influenced by nature and extremely variable, which significantly reduces their use (Abdul et al. 2022; Rahman et al. 2022). In contrast, geothermal energy is one of the clean energy sources that are unaffected by the environment, continuous and stable (Tomasini-Montenegro et al. 2017; Tosti et al. 2020). It comes from deep within the earth and has abundant reserves. Its exploitation has been widely developed in recent years (Marazuela and Alejandro 2022; Yuan et al. 2021).

To improve the efficiency of geothermal energy extraction, cementing geothermal wells is one of the most effective and simple means, which is because cementing can fully fill the pores between the casing and the wellbore, thereby accelerating the heat transfer rate between the formation and the heat exchanger. The thermal conductivity of conventional cement-based cementing materials tends to be between 0.8 and 1 W/(m·K) (Espinosa-Paredes et al. 2002; Santoyo et al. 2001; Wang et al. 2020; Won et al. 2015; Wu et al. 2020), which is much higher than 0.026 W/(m·K) of air and 0.599 W/(m·K) of water in the well without cementing (Chalermphan et al. 2018; Kadoya et al. 1985). However, it is again much lower than 2 ~ 3 W/(m·K) for underground rock formations (Macaulay et al. 2013), which is detrimental to the development of geothermal energy because it hinders the heat transfer between the formation and the heat exchanger. Therefore, it is necessary to add thermally conductive fillers to the cementing materials to create composites, so that the thermal conductivity of the materials can be maximized.

Currently, there are abundant research results on cement-based composite (CBC) for cementing geothermal wells (Kamali et al. 2021; Won et al. 2015; Xu 2014). To improve the formulation of cementing materials, Silvaa and Milestone (2018) added silica to cement to solve the problem of acid resistance of cementing materials for geothermal wells and to improve the service life of heat exchangers. Hamid et al. (2019) added a foaming agent to the cement matrix to solve the problem of easy leakage in deep geothermal wells to create a foam cement, but this inevitably reduces its thermal conductivity. Seńczuk et al. (2022) tried to add mining waste (basalt dust) to the cement matrix and applied it to cement geothermal wells. However, it was found that the thermal conductivity and compressive strength of cement stone decreased as its content increased. Yang et al. (2022) prepared a high thermal conductivity cementing material for geothermal wells using graphite, iron powder, and quartz sand, which effectively improved its thermal conductivity. These studies provide favorable technical references for the development of CBC for geothermal well cementing, but there are fewer theoretical studies on the thermal conductivity of materials and analysis of the influencing factors. Therefore, it is only possible to refer to the field of cement concrete (Espinosa-Paredes et al. 2002; Santoyo et al. 2001). Zhen et al. (2012) used the parallel hot line method to measure the thermal conductivity of cement-based materials, aggregates and mortars, and proposed a new Series–Parallel model to calculate the thermal conductivity. Xu et al. (2018) investigated the effects of interfacial thermal resistance and inclusion size on the thermal conductivity of cement-based materials based on the effective medium theory, which provided guidance for predicting the thermal properties of cementing materials. Honorio et al. (2018) estimated the heat capacity, thermal conductivity, and coefficient of thermal expansion of concrete using an analytical homogenization method. Dong et al. (2022) developed a prediction model for the thermal conductivity of cement-based materials, which can be used to predict the thermal conductivity of cementing materials

with different sand-to-cement ratio, porosity, and saturation. Although these studies can provide references for predicting the thermal conductivity of CBC, most of these models have low veracity and the focus is not on the thermal conductivity filler, which is not applicable to the field of geothermal well cementing. The current research on the thermal conductivity of CBC in geothermal wells is mostly focused on indoor tests, which inevitably requires a lot of time and cost. Therefore, it is necessary to propose an accurate mathematical and numerical model for predicting thermal conductivity, which can theoretically support the development of high thermal conductivity cementing materials and save a lot of cost and time. In addition, the analysis and control of the factors influencing the thermal conductivity of CBC can ensure the optimum thermal conductivity of the material to the maximum extent.

In this work, the microstructure and simplified model of cement-based materials was investigated through indoor tests, theoretical analysis and numerical simulation. The mathematical and numerical models were developed for predicting the thermal conductivity of CBC based on the analysis of conventional thermal conductivity calculation models. The veracity of the proposed models was verified by comparison with the experimental measurement results. The effects of shape, size, spacing of thermally conductive filler particles and curing temperature on the thermal conductivity of CBC were also investigated. The results of this study provide explain for practical engineering applications and directional guidelines for future research on similar composites.

Microstructure of cement-based materials

Cement-based materials are usually produced by hydration of cement clinker particles. Usually, cement clinker is mainly composed of tricalcium silicate (Ca_3SiO_5, C_3S), dicalcium silicate (Ca_2SiO_4, C_2S), tricalcium aluminate ($3CaO{\cdot}Al_2O_3$, C_3A), tetracalcium iron aluminate ($4CaO{\cdot}Al_2O_3{\cdot}Fe_2O_3$, C_4AF), and so on. When mixed with water, they undergo rapid hydration reactions to form hydration products including $Ca(OH)_2$, calcium aluminate ($3CaO{\cdot}Al_2O_3{\cdot}3CaSO_4{\cdot}32H_2O$, AFt), and hydrated calcium sulfoaluminate ($Ca_5Si_6O_{16}(OH){\cdot}4H_2O$, C-S-H) (Kurumisawa et al. 2013). These hydration products have different morphologies, complex structures, and heterogeneous mixing, resulting in cementing materials with high heterogeinity. This is the main difference between cementing materials and other materials, such as metals or polymers (Alexander and Sergey 2022).

To accurately study the macroscopic physical properties of cement-based materials, it is necessary to first analyze the microstructure of the materials. In this paper, a commonly used G-grade oil well cement (from Shandong Shengwei Cement Plant, China), whose chemical composition determined by X-ray Fluorescence Spectrometer (XRF) is shown in Table 1, was selected as the cementing specimen of study. The cement slurry was prepared with a water-cement ratio of 0.4 and kept at 25 ℃ for 28 days to allow complete hydration, and cement stone samples were obtained.

Subsequently, during the testing of samples, all parameters were obtained by averaging the results of not less than three tests. The maximum error of these three groups of tests should not exceed 5%. If the data have a large error, it should be removed and retested until the results of at least three groups of tests meet the requirements.

Table 1 Chemical composition of G-grade oil well cement determined by XRF. (wt%)

Composition	Oxides							Minerals			
	CaO	SiO_2	Fe_2O_3	Al_2O_3	MgO	K_2O	Na_2O	C_3S	C_2S	C_3A	C_4AF
Average	63.32	21.0	5.98	4.28	1.99	0.21	0.14	55.14	18.62	1.13	18.18
Maximum	63.49	21.4	6.07	4.37	2.05	0.26	0.19	55.61	19.01	1.22	18.36
Minimum	63.18	20.5	5.86	4.21	1.91	0.18	0.11	54.88	18.28	1.05	17.85
Standard deviation	0.16	0.46	0.11	0.08	0.07	0.04	0.04	0.41	0.37	0.09	0.29

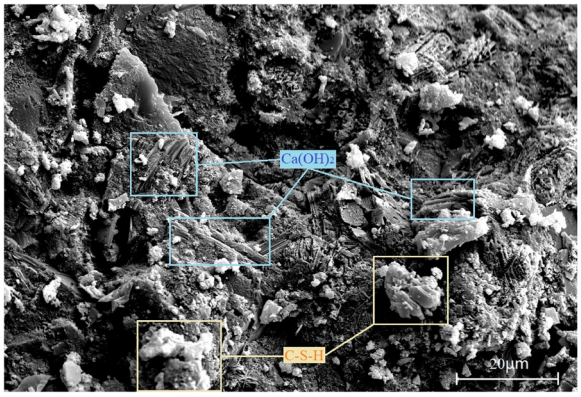

Fig. 1 Micromorphology of cement-based materials determined by SEM

Micromorphology

A cement stone sample with a size of 1 cm^3 was collected, polished, and sprayed with gold. Its microscopic morphology was observed using a JSM-IT500 scanning electron microscope, as shown in Fig. 1. It indicates that the clinker particles in cement stone have undergone sufficient hydration with a large amount of plate-like $Ca(OH)_2$ and agglomerated C-S-H generation. The hydration product particles are filled with a large number of needle-like AFt between them, and the interconnections are relatively tight. The overall structure of cement stone is relatively dense, and there are no obvious large pores. However, some small amorphous particles can be seen with surfaces covered with C-S-H. These particles may be clinker bodies still in the process of hydration. This indicates that the hydration of the cement is not complete. This is because the hydration of cement is an extremely long process, and the hydration process is extremely complex and involves many reactions (Kong et al. 2016). It is generally believed that after 28 d, the main clinker particles are hydrated, and the remaining part will continue to undergo hydration reactions at different rates depending on temperature and water, etc. in different application environments (Pelletier et al. 2010).

Component analysis

A cement stone sample with a size of 0.5 cm^3 was collected and ground to a particle size of less than 80 μm. Its phase components were examined using an XRD-6100 X-ray diffractometer, as seen in Fig. 2. Since $Ca(OH)_2$ and C_3S are crystalline phases, that can be easily detected by XRD, whereas C-S–H which is a non-crystalline phase cannot be

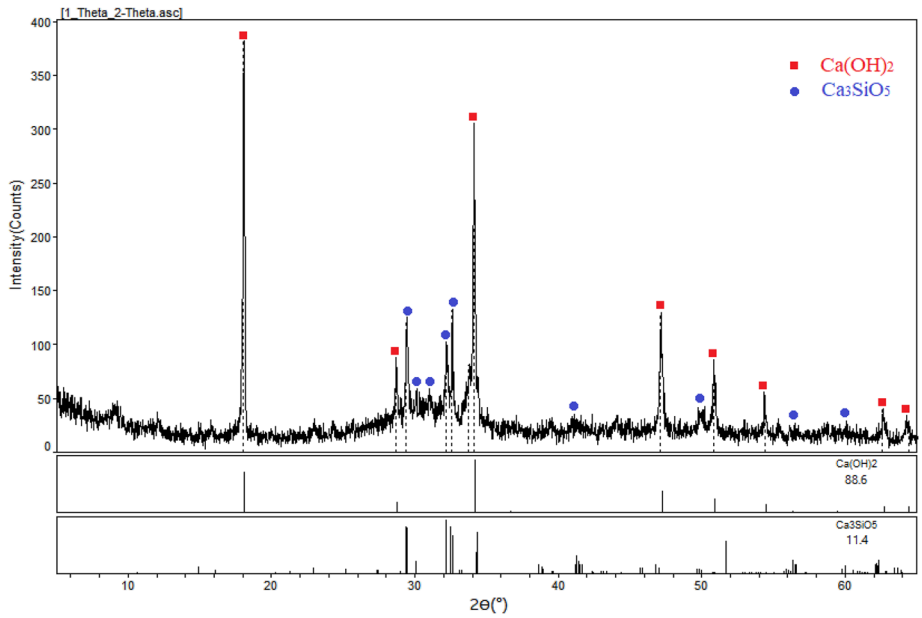

Fig. 2 XRD difractogram showing the phase components of cement-based materials

easily detected. Therefore, the degree of hydration of cement stone was mainly characterized by the relative contents of $Ca(OH)_2$ and C_3S. As shown in Fig. 2, the diffraction peaks of $Ca(OH)_2$ in cement stone have high peaks and their characteristics are very obvious. In contrast, the diffraction peaks of C_3S are not obvious and have low peaks. The relative contents of $Ca(OH)_2$ and C_3S are 88.6% and 11.4%, respectively, indicating that $Ca(OH)_2$ is highly developed compared to C_3S. It shows a high degree of hydration of cement stone, which can be expressed by the relative content of $Ca(OH)_2$, i.e., a hydration rate of 88.7%. The reason why the hydration rate did not reach 100% is that cement can take several years to hydrate (Land and Stephan 2015). On the other hand, it is because some of the hydration products are wrapped around the surface of the clinker particles, preventing them from contacting water and thus limiting their hydration reactions (Lupyana et al. 2022).

Development and validation of thermal conductivity model

The generation and propagation of heat is usually through the vibration of electrons, molecules, or phonons. Among these, electrons propagate at a very fast rate, as in metallic materials, which have a high thermal conductivity. However, non-metallic materials have no electrons. Heat propagates in it only by phonons at a slow rate. Therefore, it tends to have lower thermal conductivity (Farzadian et al. 2022). The thermal conductivity is an important parameter to describe the thermal conductance of a material. At present, there are relatively few reports on the calculation model of thermal conductivity of CBC (Burger et al. 2016; Yu et al. 2016). But the relevant research can refer to the models of filled composites in the field of polymer materials, and the more applied ones are Series–Parallel model (Jia et al. 2020), Maxwell–Eucken model (Zhang et al. 2017), and the effective medium theory model (Pang et al. 2014).

Thermal conductivity model for filled composites

Series–Parallel model

The Series–Parallel model (SP model) was proposed by Deissler and Boegli (Tarnawski and Leong 2012). They equated heat transport in the composite with electrical transport through series and parallel structures in the circuit, and equated the matrix and filler as two components. The matrix and filler are in close contact and both are oriented perpendicular to the heat flow direction in the Series model and parallel to the heat flow direction in the Parallel model (Jia et al. 2020). The Series and Parallel models are shown in Eqs. (1) and (2), respectively. While this model considers the impact of the matrix and filler on the composite's thermal conductivity, it oversimplifies the situation by treating the filler and matrix as independent components. This approach does not reflect the actual distribution of fillers within the material, which limits its veracity and applicability (Kang and Ge 2015).

$$\frac{1}{k_s} = \frac{1-\varphi_f}{k_m} + \frac{\varphi_f}{k_f} \tag{1}$$

$$k_P = \left(1-\varphi_f\right) \cdot k_m + \varphi_f \cdot k_f \tag{2}$$

where k_s, k_P are the thermal conductivity of the composite in the Series and Parallel models, respectively, W/(m·K); k_m, k_f are the thermal conductivity of the matrix and filler, respectively, W/(m·K); ϕ_f is the volume fraction of the filler, vol%.

Maxwell–Eucken model

The Maxwell–Eucken model (ME model) is based on the conductivity equation obtained by Maxwell by solving the Laplace equation (Maxwell 1873), which Eucken obtained by replacing the electrical conductivity of the composite with the thermal conductivity (Zhang et al. 2017), as shown in Eq. (3). The veracity of this model is higher than that of the SP model because it assumes that the fillers are uniformly distributed in the matrix and are closer to the true state of the composite material. However, its applicability is limited because it is only more effective when the fillers are spherical and the content is less than 20 vol %. Additionally, this model does not consider the interaction between the filler particles, which is why it is also referred to as the 'island model' (Chen et al. 2023).

$$k_{ME} = k_m \cdot \frac{k_f + 2k_m - 2\varphi_f\left(k_m - k_f\right)}{k_f + 2k_m + \varphi_f\left(k_m - k_f\right)} \tag{3}$$

where k_{ME} is the thermal conductivity of the composite in the ME model, W/(m·K).

Effective medium theory model

The effective medium theory model (EMT model) assumes that both filler and matrix can be continuous phases, and whether they are or not depends on the relative content of both (Pang et al. 2014; Xu et al. 2018). As shown in Eq. (4). The EMT model differs from the SP and ME models in that it considers the filler and matrix as a whole, rather

than two independent parts, which makes it more accurate in theory. However, Eq. (4) shows that this model only accounts for one filler and matrix, making it unsuitable for complex composites made up of multiple fillers (Gong et al. 2014). As a result, this model's applicability is also limited.

$$k_{EMT} = \frac{1}{4}\left[k_f(3\varphi_f - 1) + k_m(2 - 3\varphi_f) + \sqrt{\left[k_f(3\varphi_f - 1) + k_m(2 - 3\varphi_f)\right]^2 + 8k_f k_m}\right] \tag{4}$$

where k_{EMT} is the thermal conductivity of the composite in the EMT model, W/(m·K).

Thermal conductivity model of CBC

The above models provide theoretical support for calculating the thermal conductivity of composites composed of a single filler and a homogeneous matrix. However, for cement-based materials, the matrix is composed of hydration products and unhydrated clinker, which is a complex mixed system rather than homogeneous, thus the above theories cannot be accurately applied to the CBC system. Therefore, the properties of the CBC system require a new model for calculating its thermal conductivity.

Mathematical model

From the results of "Component analysis" section it is clear that the cement matrix reaches 88.6% hydration after full hydration (28 d), with 11.4% of unhydrated clinker. It is possible to simplify this cement system into a composite material consisting of two structural layers, the hydrated and the unhydrated layer, respectively. Among them, the content of hydration products is much higher than that of unhydrated clinker, so the hydration products are considered as the matrix and the unhydrated clinker as the filler. Since the hydrated products and the unhydrated clinker are in close contact or wrapped around each other, they can be perpendicular to the heat flow in all directions, which is more consistent with the assumption made by the Series model. Therefore, the thermal conductivity model of a single cement-based material can be obtained by the Series model, as shown in Eq. (5).

$$k_c = \frac{k_h \cdot k_u}{k_u(1 - \varphi_u) + k_h\varphi_u} \tag{5}$$

where k_c, k_h, k_u are the thermal conductivities of the single cement-based materials, hydration products and unhydrated clinker, respectively, W/(m·K); ϕ_u is the volume fraction of unhydrated clinker, vol%.

Equation (5) fully takes into account the contribution of cement clinker and hydration products to the thermal conductivity of cement stone, and does not regard cement stone as a single homogeneous material, but as a two-part composition of hydrated and non-hydrated substances, which is more realistic. However, in the case of geothermal wells, it is necessary to add high thermal conductivity fillers to the cement to improve the thermal conductivity of CBC. Apparently, Eq. (5) cannot accurately calculate the thermal conductivity of CBC because it does not account for the influence of thermally conductive fillers. At this point, CBC can be considered as a binary composite system consisting of a cement matrix and a thermally conductive filler. The thermally conductive fillers are

mostly spherical in shape. They are usually low in content and tend to be scattered. As a result, CBC is more consistent with the assumptions of the ME model. Therefore, the thermal conductivity model of CBC can be obtained by combining the ME model, see Eq. (6).

$$k_T = k_c \cdot \frac{k_f + 2k_c - 2\varphi_f\left(k_c - k_f\right)}{k_f + 2k_c + \varphi_f\left(k_c - k_f\right)} \tag{6}$$

where k_T is the thermal conductivities of CBC, W/(m·K).

Substituting Eq. (5) into Eq. (6) to obtain Eq. (7):

$$k_T = \frac{k_h \cdot k_u}{k_u(1-\varphi_u) + k_h\varphi_u} \cdot \frac{k_f + 2\frac{k_h \cdot k_u}{k_u - k_u\varphi_u + k_h\varphi_u} - 2\varphi_f\left(\frac{k_h \cdot k_u}{k_u - k_u\varphi_u + k_h\varphi_u} - k_f\right)}{k_f + 2\frac{k_h \cdot k_u}{k_u - k_u\varphi_u + k_h\varphi_u} + \varphi_f\left(\frac{k_h \cdot k_u}{k_u - k_u\varphi_u + k_h\varphi_u} - k_f\right)} \tag{7}$$

Simplifying Eq. (7) to obtain Eq. (8):

$$k_T = \frac{\left(2k_h + k_f\right)k_u + (k_h - k_u)k_f\varphi_u + 2\left(k_f\varphi_u - k_h\varphi_f\right)k_u + 2(k_h - k_u)k_f{\varphi_u}^2}{\left(\frac{1}{k_h} - \frac{\varphi_u}{k_h} + \frac{\varphi_u}{k_u}\right)\left[\left(2k_h + k_f\right)k_u + \left(k_h - k_f\right)k_u\varphi_f + k_f\varphi_u(k_h - k_u)\left(1 - \varphi_f\right)\right]} \tag{8}$$

According to the findings of Qomi et al. (2015), the thermal conductivity of hydrated product is 1.15 W/(m·K), and the thermal conductivity of unhydrated clinker is 3.4 W/(m·K). Substituting them into Eq. (8), k_h and k_u can be eliminated. Finally, after simplification, the mathematical model of the thermal conductivity of CBC can be obtained, which is shown in Eq. (9).

$$k_T = \frac{7.82 + 3.4k_f + 4.55k_f\varphi_u - 7.82\varphi_f - 4.5k_f{\varphi_u}^2}{(0.87 - 0.576\varphi_u) \times \left[7.82 + k_f(3.4 - 2.25\varphi_u)\left(1 - \varphi_f\right) + 3.91\varphi_f\right]} \tag{9}$$

Numerical model

The above mathematical modeling process shows that the cement matrix can be divided into two parts, the hydrated layer and the unhydrated layer, and it is more consistent with the Series model. Therefore, the three-dimensional solid model of the cement matrix can be established using COMSOL Multiphysics software, as shown in Fig. 3.

To simplify the model and reflect the actual situation as much as possible, the following assumptions are made: (1) Each part of the model is isotropic; (2) The heat propagation is one way, i.e., from the top of the model to the bottom; (3) The heat propagation follows the law of thermodynamics; (4) The heat propagation occurs only within the model and is not affected by the external temperature. Based on these assumptions, the cement matrix is set as a cube with a side length of 10 cm. The built-in solid heat transfer module of the software is used for numerical simulation. The calculation method is shown in Eq. (10). The initial temperature is set to 293.15 K. The top surface is set to the 'Heat Flux' boundary condition, and the heat flux size is set to 1050 W/m^2. The bottom surface is set to the 'Temperature' boundary condition, and the temperature is set to 273.15 K. The model mesh is set to a more refined 'Free Tetrahedral Mesh'. The steady-state model is used to calculate the temperature. Based on the temperature difference

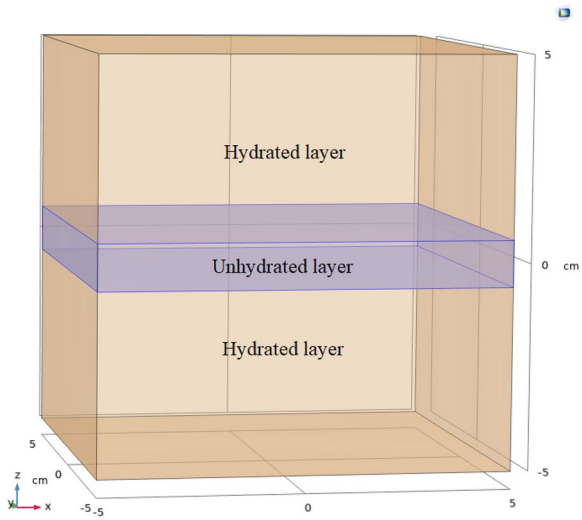

Fig. 3 Three-dimensional solid model of the cement matrix

between the upper and lower surfaces, the numerical solution of the thermal conductivity of CBC can be obtained using Fourier's law, as shown in Eq. (11).

$$\rho c_p u \cdot \nabla T + \nabla \cdot q = Q \tag{10}$$

$$q = -k \cdot \nabla T \tag{11}$$

where ρ is the density, kg/m^3; c_p is the constant pressure specific heat capacity, J/(kg·K); u is the velocity, m/s; ∇T is the temperature gradient, and the negative sign indicates that the heat flow direction is opposite to the temperature gradient direction; q is the heat flow density, W/m^2; Q is the heat source, W/m^3; and k is the thermal conductivity, W/(m·K). In addition, it is necessary to compare the model calculation results with the experimental results to verify the veracity of the model. The relevant contents will be explained in detail in "Comparative verification of thermal conductivity models" section.

Comparative verification of thermal conductivity models

The veracity of the above mathematical and numerical models was verified by experiments. Graphite with a thermal conductivity of 151 W/(m·K) was selected as the thermally conductive filler. Graphite with volume fractions of 2.5–30 vol% was added to the cement base in 2.5 vol% increments, respectively, and the cement stone samples were obtained by standard curing for 28 d under 25 ℃ conditions. The surface of the cement stone was dried, and its thermal conductivity was tested by a DRE-2C type thermal conductivity tester, which is based on the transient plane heat source method with a testing range of 0.01 to 100 W/(m·K) and the experimental accuracy is precise up to the fourth decimal point with an accuracy range of ± 5%. The thermal conductivity of the pure cement stone was 1.18 W/(m·K). For better comparison with the established model, the volume fraction is needed as an indicator of the content. The operation of weighing the graphite volume in the test is extremely difficult due to the powder form of graphite. To facilitate the operation, it is necessary to convert the volume fraction into a weight

fraction for the purpose of determining the content by weighing the graphite mass. The calculation of converting the volume fraction to the weight fraction is shown in Eq. (12).

$$\omega = \frac{\rho_f}{\rho_m} \cdot \varphi \tag{12}$$

where ω is the weight fraction, wt%; ρ_f is the density of graphite, kg/m^3; ρ_m is the density of cement matrix, kg/m^3, and ϕ is the volume fraction, vol%.

The thermal conductivity of graphite and pure cement stone is 151 W/(m·K) and 1.18 W/(m·K), respectively. The volume fraction of unhydrated clinker is 11.4 vol%. These values and the different volume fractions of graphite are substituted into the Series model, ME model, EMT model, mathematical model, and numerical model to calculate. The results are presented in Fig. 4. In addition, to more intuitively and accurately evaluate the consistency between the calculation results of each model and the experimental results, the merit function shown in Eq. (13) was used to quantitatively analyze the deviation between them.

$$N = \sqrt{\frac{\int_{\lambda_1}^{\lambda_f} (E(\lambda) - S(\lambda))^2 d\lambda}{\left(\int_{\lambda_1}^{\lambda_f} E(\lambda) d\lambda\right)^2}} \tag{13}$$

where $E(\lambda)$ is the experimental test result; $S(\lambda)$ is the model calculation result; N is the deviation value between the results. Besides, the smaller the value of N, the better the fitting degree between the model and the experiment and the higher the veracity of the model. This merit function has been widely used due to its quantitative assessment for model veracity (Andaverde et al. 2019; Estrada-Wiese et al. 2018; Molina-Rodea and Wong-Loya 2021).

It evidences that the thermal conductivity of CBC shows a continuous increasing trend with increasing filler content. The N values between the calculation results of the mathematical, numerical, Series, ME and EMT models and the experimental test results

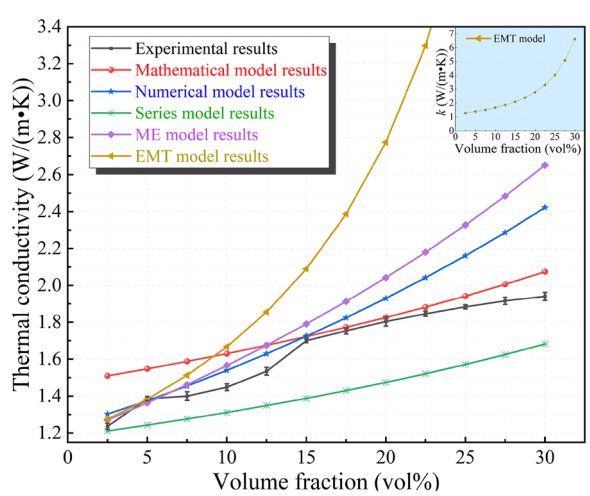

Fig. 4 Comparison of the thermal conductivity of each model with different volume fractions of fillers

were 0.0237, 0.0294, 0.0694, 0.1114 and 0.2302, respectively. Hence one can see that the N values of the mathematical and numerical models established in this paper are the smallest and closest compared to other models, which indicates that the mathematical and numerical models have less error and are closer to the measured values with higher veracity compared to the Series, ME and EMT models. Among them, the mathematical model is closer to the measured value when the filler content is greater than 15 vol%, and the calculated result is slightly larger than the measured value when the content is less than 15 vol%. The numerical model is closer to the measured value when the filler content is less than 15 vol%, and the calculated result is slightly larger than the measured value when the content is greater than 15 vol%. The reason may be that the mathematical model considers the influence of both thermally conductive filler and unhydrated clinker in the construction process, where the content of unhydrated clinker is 11.4 vol%. When the filler content is low, the influence of the unhydrated clinker is greater, while its thermal conductivity is much higher than that of the cement matrix. This leads to high overall thermal conductivity of the material when the filler content is low. When the filler content is higher, the influence of the unhydrated clinker is less and the results are closer to the measured values. The numerical model was built by simplifying the filler as a sphere with different diameters, without considering the heat loss such as scattering at the filler interface. When the filler content is small, the heat loss by scattering is smaller because the filler particles are smaller, so the numerical simulation results are closer to the actual ones. However, as the filler content increases, the particle interface becomes larger and the heat loss due to scattering increases. So the actual results are small, but the simulated results are large.

In summary, a mathematical model can be selected for low filler content and a numerical model can be selected for high filler content when predicting and calculating the thermal conductivity of CBC. That provides a more reasonable choice for accurately predicting the thermal conductivity of CBC, which can save a lot of testing cost and time.

Analysis of factors influencing thermal conductivity

CBC for geothermal well cementing is mainly composed of cement matrix and filler, so its thermal conductivity is also mainly influenced by the filler and cement matrix. Among them, the influence of the filler is related to the shape, diameter and spacing of the particles in addition to the content (as seen in "Comparative verification of thermal conductivity models" section) (Asadi et al. 2018; Honorio et al. 2018). In contrast, the cement matrix is mainly influenced by the hydration process, which is inextricably linked to temperature. Coupled with the fact that the geothermal well is a continuous high-temperature environment, this may have a significant impact on the thermal conductivity of CBC (Seungmin 2015).

Effect of filler shape on thermal conductivity

Graphite was selected as the thermally conductive filler and its volume content was controlled to 20 vol%. The filler shapes were set as cube, sphere and plate (vertical heat flow direction and parallel heat flow direction, respectively). The effect of filler shapes on the thermal conductivity of CBC is investigated by the numerical model established in "Thermal conductivity model of CBC" section. The results of the thermal conductivity of

Table 2 Thermal conductivity of CBC with different filler shapes

Filler shapes	Upper surface temperature T_1/K	Lower surface temperature T_2/K	Temperature difference ΔT/K	Thermal conductivity k/W•(m•K)$^{-1}$
Cube	321.84	274.40	47.44	2.11
Sphere	326.30	274.51	51.79	1.93
Plate (vertical heat flow)	340.92	274.89	66.03	1.51
Plate (parallel heat flow)	291.14	273.61	17.53	5.70

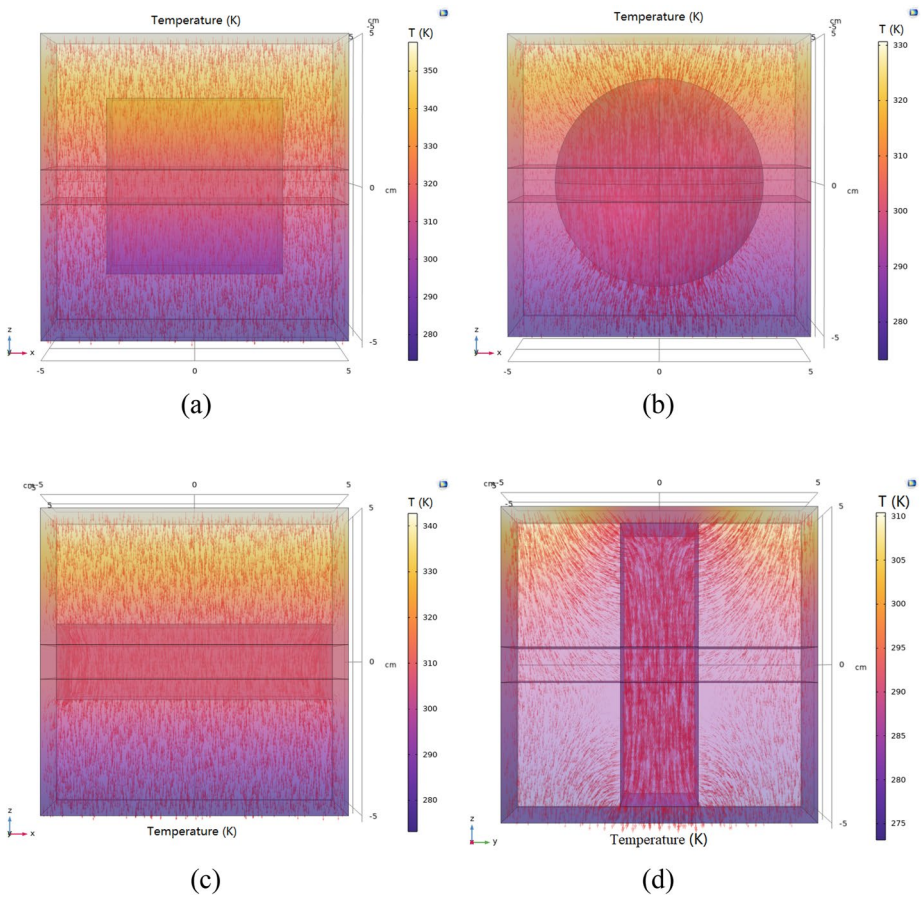

Fig. 5 Heat flow distribution in CBC with different filler shapes. **a** Cube, **b** Sphere, **c** Plate (vertical heat flow), **d** Plate (parallel heat flow)

the materials with different filler shapes are shown in Table 2, and the heat flow distribution is shown in Fig. 5. It suggests that the cubic filler is more beneficial in improving the thermal conductivity of the material compared to the spherical filler. The plate filler has obvious anisotropy. The thermal conductivity of the material is maximum when parallel to heat flow, but minimum when perpendicular to heat flow. This is because the heat flow only needs to pass through the top and bottom surfaces of the cubic filler when it passes through it, but it needs to pass through all surfaces when it passes through the spherical filler, as shown in Fig. 6a, b. For the same volume, the surface area of the sphere is much larger than the top and bottom surfaces of the cube. As a result, the thermal conductivity

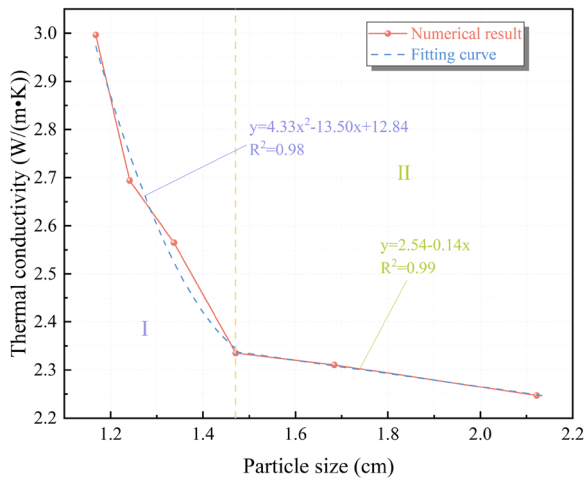

Fig. 6 Variation curve of thermal conductivity with filler particle size

of the material is reduced because the interfacial thermal resistance and scattering effect are greater when heat passes through the spherical particles than through the cubes. For the plate filler, as seen in Fig. 6c, b, when it is parallel to the heat flow, heat preferentially propagates through the filler very quickly, so the thermal conductivity of the material is very large. If it is perpendicular to the heat flow, on one hand it has a very large upper and lower surface area, which causes a large interfacial thermal resistance. On the other hand, it has a small thickness in the direction of the heat flow, which results in the heat also having to travel through a long section of the cement matrix, so that the thermal conductivity of the material is minimal.

It signals that the shape of the filler plays a role mainly by changing the contact state of the particles. When selecting thermally conductive fillers in practical engineering, square fillers can be preferred. This allows them to form face-to-face contact, maximizing the thermal conductivity of CBC. The spherical fillers tend to form only point contact, which is unfavorable for heat propagation. In addition, when choosing graphite, graphene, carbon fiber and other thermally conductive fillers with plate, sheet or rod structure, because they have obvious anisotropy, how to control their distribution direction in the matrix is the key to improve the overall thermal conductivity of the material.

Effect of filler particle size on thermal conductivity

Since cubic thermal conductive fillers are rare in practical applications but spherical filler particles, such as iron powder, copper powder, and carbon powder, are more common, the shape of the filler has been set to be spherical to better reflect the actual situation. To investigate the effect of filler particle size on the thermal conductivity of CBC, it is necessary to control the filler content. Thus, the volume fraction of the filler was set to 20 vol% and then the particle size was controlled by changing the number of filler particles. To facilitate simulation and analysis, the number of filler particles was set to 5, 10, 15, 20, 25 and 30, respectively, and the corresponding particle radius were 2.122 cm, 1.684 cm, 1.471 cm, 1.337 cm, 1.2413 cm and 1.168 cm. The particles were in close contact with each other and all other conditions were controlled to be

the same. The effect of filler particle size on the thermal conductivity of CBC was investigated by numerical modeling. The results are shown in Fig. 6. It expresses that the overall thermal conductivity of CBC shows two stages of rapid decrease and then slow decrease with the increase of filler particle size, which correspond to the I and II regions in Fig. 6, respectively. In the I and II stages, the thermal conductivity of CBC decreases in power series and linear form, respectively, and their fitted equations are shown in Eqs. (14) and (15).

$$k_I = 4.33r^2 - 13.5r + 12.84;\ R^2 = 0.98 \tag{14}$$

$$k_{II} = 2.54 - 0.14r;\ R^2 = 0.99 \tag{15}$$

where, k_I and k_{II} are the thermal conductivity of CBC in stages I and II, respectively, W/(m·K); r is the filler particle size, cm; R^2 is the fitting degree, and the closer its value is to 1, the better the fitting effect. It can be seen from Eqs. (14) and (15) that the R^2 of the fitting equations of stage I and II are 0.98 and 0.99, respectively, which indicates that the fitting results are reliable.

The reason for the above phenomenon is that with the same filler content, the larger the particle size, the smaller the number of particles, and the fewer the heat conduction paths formed by the particles in contact with each other, as shown in Fig. 7. When the filler particle size is 1.168 cm, as shown in Fig. 7a, the thermal conduction paths are very numerous, and the heat propagates almost exclusively through the thermally conductive filler at a very fast rate. Therefore, the thermal conductivity of the material is very high. As the particle size increases to 1.471 cm, as shown in Fig. 7b, the number of filler particles decreases from 30 to 15, at which time the thermal conductivity paths decrease rapidly and the distribution area of the heat flow in the matrix increases significantly, so the thermal conductivity of the material decreases rapidly. When the particle size continues to increase to 2.122 cm, as shown in Fig. 7c, at this time, although the thermal conductivity paths continue to decrease, the distribution area of the heat flow in the matrix does not change much compared to Fig. 7b. At this point, the increase in thermal conductivity of the material has been relatively weak due to the small number of thermal conductivity paths. Therefore, the rate of decrease in thermal conductivity becomes very slow. It declares that the particle size of the filler mainly affects the thermal conductivity of CBC by changing the number of thermal conduction paths. In practical engineering, when the filler content

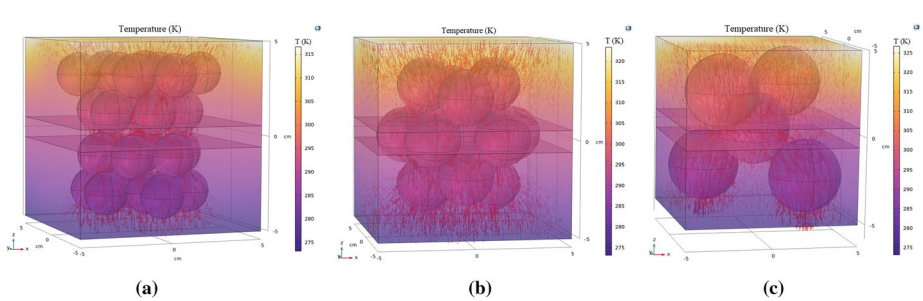

Fig. 7 Heat flow distribution of CBC with different particle sizes of fillers. (**a**) $r = 1.168$ cm; (**b**) $r = 1.471$ cm; (**c**) $r = 2.122$ cm

is high (capable of forming thermal conductivity paths), the use of smaller particle size of thermal conductivity filler as much as possible will help to further improve the overall thermal conductivity of the material.

Effect of filler particle spacing on thermal conductivity

The filler was set to be spherical with a volume fraction of 20 vol%. The number of particles was set to 8. The particle size was set to 1.8139 cm. The filler particles were uniformly distributed in the center of the body of the CBC. The particle spacing was controlled by a mirror-image operation. All other conditions were controlled the same. The particle spacing was changed from 0 cm to 2.5 cm. The effect of the filler particle spacing on the thermal conductivity of the CBC was investigated by numerical modeling. The results are shown in Fig. 8.

It manifests that the trend of thermal conductivity of CBC with the increase of filler particle spacing can be divided into three stages, as indicated by stages I, II and III in Fig. 8. Among them, the range of particle spacing in stage I is 0 ~ 0.08 cm. The thermal conductivity of the material gradually decreases with increasing spacing. This is because when the filler particles are in contact with each other, the filler is a continuous phase, which will form thermal conductivity paths, and heat will preferentially propagate through these paths. As soon as the particles are separated, these paths are destroyed, resulting in an instantaneous decrease in thermal conductivity. The thermal conductivity of the material increases slowly as the particle spacing gradually increases and at stage II. The spacing range at this stage is 0.08–0.8 cm. This is because when the filler spacing is small and there is no mutual contact, the thermal conductivity path is not formed at this time, and the degree of interaction between the particles is greater. The heat is refracted and scattered many times between the particle interfaces, causing heat loss. This phenomenon can be called the 'agglomeration effect'. As the spacing gradually increases, the bond between the particles weakens and the heat loss between the interfaces decreases, resulting in a small increase in the thermal conductivity of the material. As the particle spacing continues to increase to greater than 0.8 cm (stage III), the thermal conductivity

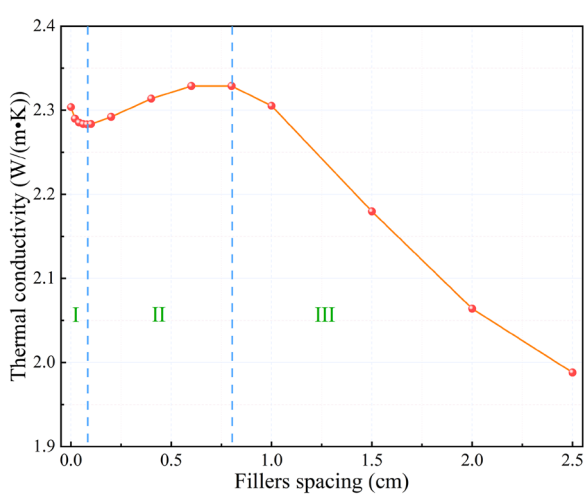

Fig. 8 Variation curve of thermal conductivity with filler spacing

decreases with increasing spacing. This is because as the packing spacing increases to a distance greater than its own radius, the packing particles gradually become distributed in 'islands'. The connection between the particles becomes weaker and weaker as the spacing increases, resulting in a decreasing probability that heat will be attracted to a packing particle after passing through another. More and more heat must travel slowly through the matrix. Thus, the overall thermal conductivity of the material continues to decrease. It implies that the spacing of filler particles mainly affects the thermal conductivity of CBC by changing the interfacial thermal resistance between particles. In practical engineering applications it would be more beneficial to improve the thermal conductivity of the composite material if the spacing of the filler particles could be better controlled around their radius size. Obviously, that is very difficult. In addition, it would be advantageous to keep the filler particles as small as possible while avoiding their agglomeration.

Effect of curing temperature on thermal conductivity

Graphite at 5 vol% was added to the cement matrix. They were kept at 20 ~ 180 ℃ in 20 ℃ increments for 28 days to fully hydrate and then removed to obtain cement stone samples. Their thermal conductivity was tested and the results are shown in Fig. 9. It proclaims from the figure that the thermal conductivity of CBC showed a trend of rapid increase followed by up-and-down fluctuation with the increase of curing temperature. For convenience of description, it is divided into five stages, which are shown in Fig. 9 from stage I to V. In stage I, the temperature increases from 20 ℃ to 100 ℃, and the thermal conductivity of the material increases from 1.386 W/(m·K) to W/(m·K), which is an increase of 7%. And there is a quadratic positive correlation between the thermal conductivity of CBC and temperature between 20 and 80 ℃. The temperature range of stage II is 100–120 ℃, and the thermal conductivity decreases from 1.483 W/(m·K) to 1.452 W/(m·K), which is a decrease of 2%. The temperature range of stage III is 120 ~ 140 ℃, and the thermal conductivity increases by 0.76%. The temperature range of stage IV is 140 ~ 160 ℃, and the thermal conductivity decreases by 1.71%. When the temperature is higher than 160 °C (stage V), the thermal conductivity basically stabilizes.

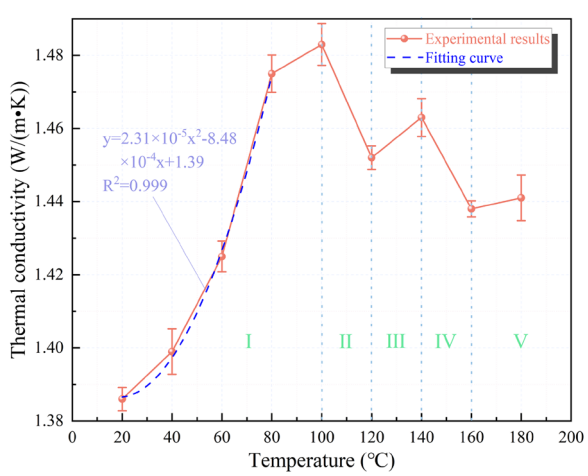

Fig. 9 Variation curve of thermal conductivity with temperature

To investigate the causes of the above phenomenon, the cement stone samples kept at 20 ℃, 100 ℃ and 180 ℃ were selected and examined by SEM, and the results are shown in Fig. 10. By comparison, it makes clear that when the temperature is low (20 ℃), as shown in Fig. 10a, some thick layers of $Ca(OH)_2$ and agglomerated C-S–H are formed inside the CBC. But the $Ca(OH)_2$ content is low and the C-S–H is wrapped around the particle surface, indicating that some of the clinker particles may still be hydrating at this time. The overall hydration of the material was insufficient. When the temperature was increased to 100 ℃, as shown in Fig. 10b, the C-S–H content in the material decreased and a large number of small pieces of $Ca(OH)_2$ appeared, and the material as a whole was more dense than that at 20 ℃. It can throw light on that the degree of hydration of the material is higher at this temperature. When the temperature was further increased to 180 ℃, as shown in Fig. 10c, it the overall structure of the material is more lax at this time. The content of $Ca(OH)_2$ in the thick plate form is less. The C-S-H content increased significantly and the shape changed from agglomerate to flocculent. This indicates that secondary hydration may have occurred within the material at this time, resulting in a decrease in the overall structural properties of the material. This is because at low temperatures, the hydration products of cement-based materials are mainly CSH(II), $Ca(OH)_2$, AFt and AFm. When the temperature reaches 110 ℃, some of the CSH(II) will undergo secondary hydration reactions and be converted to C_2SH. When the temperature reaches about 150 ℃, almost all of the CSH(II) is converted to C_2SH (Ivan and Jan 1973). C_2SH is not as stable as CSH(II) and, therefore, leads to the degradation of the overall properties of the material (Tan and John 2004). The main chemical reactions of the whole process are shown in Eq. (16) (Razak and Sajedi 2011). This explains very well the decrease in thermal conductivity of the material in stages II and IV in Fig. 9.

$$\left\{\begin{matrix} C_3S \\ C_2S \end{matrix}\right\} + H_2O \xrightarrow{25\sim80^\circ C} \left\{\begin{matrix} Ca_2SiO_4 \cdot 3H_2O \\ Ca(OH)_2 \end{matrix}\right\} \xrightarrow{80\sim110^\circ C} \left\{\begin{matrix} Ca_2SiO_4 \cdot 3H_2O \\ Ca_2SiO_4 \cdot 2H_2O \\ Ca_3Si_2O_7 \cdot 3H_2O \\ Ca(OH)_2 \end{matrix}\right\} \xrightarrow{110\sim200^\circ C} \left\{\begin{matrix} Ca_2SiO_4 \cdot H_2O \\ Ca(OH)_2 \end{matrix}\right\} \tag{16}$$

It makes known that the influence of ambient temperature on the thermal conductivity of CBC is mainly carried out by changing the type and microstructure of hydration products of CBC. As the development of geothermal energy gradually moves deeper (> 3000 m), the temperature at the bottom of the wells will exceed 110 ℃ (based on a geothermal gradient of 3 ℃/hm) (Macenić et al. 2020). At this point, the high temperature at the bottom of the well will inevitably cause damage to the structure of the CBC, resulting in a decrease in its thermal conductivity. In practice, to avoid such a situation,

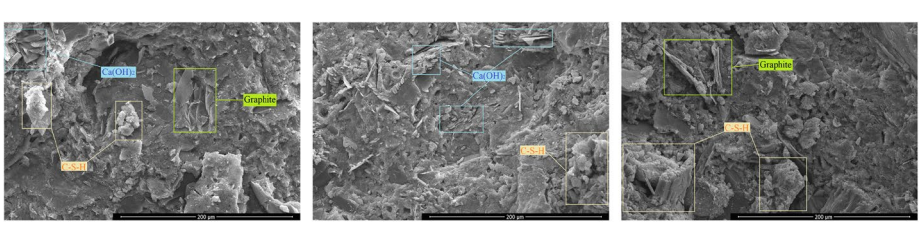

(a) (b) (c)

Fig. 10 Microstructure of CBC at different curing temperatures. (**a**) 20 °C, (**b**) 100 °C, (**c**) 180 °C

it is necessary to add high temperature resistant materials or high temperature activators to the cement-based material to increase its high temperature resistance (Ren et al. 2023). In this case, materials such as silica fume and industrial slag with high reactivity at high temperatures are the best choices (Chen et al. 2023; Powmrshelm and Clifton 1979). It can be seen that the research and development of high temperature resistant and high thermal conductivity cementing materials will play an important role in the efficient development of deep geothermal energy in the future.

Conclusion

(1) The microstructure of conventional cement-based material was studied and it was divided into a two-layer structure of hydrated and unhydrated layers. The thermal conductivity models of existing filled composites were analyzed, and it was found that the single cement-based material corresponds to the Series model and the CBC material corresponds to the ME model. Based on this, the mathematical model for thermal conductivity calculation of CBC was established by coupling the Series model and the ME model. And the corresponding numerical model was established. By comparing with the Series model, ME model, EMT model and experimental test results, it is found that the established mathematical model and numerical model are closer to the measured results and more accurate.

(2) The effects of shape, diameter, spacing of filler particles and curing temperature on the thermal conductivity of CBC were investigated. The cubic filler was found to be more favorable than the spherical filler in improving the thermal conductivity of the material. The plate filler has an obvious anisotropy. The thermal conductivity of the material tends to decrease rapidly and then slowly as the particle size of the filler increases. The thermal conductivity of the material first decreases and then increases slowly and then decreases rapidly with the increase of the particle spacing. The thermal conductivity increases rapidly, then fluctuates up and down, and finally stabilizes with the increase in curing temperature.

(3) It is suggested that cubic fillers should be preferred in engineering applications. When using graphite, graphene, carbon fiber and other fillers with plate, sheet or rod structure, the direction of their distribution in the material should be controlled. As far as possible, the use of smaller particle size of the thermal conductivity filler, while controlling the filler particles to maintain a small spacing and avoid their agglomeration, will be more conducive to improving the thermal conductivity of the material. When cementing geothermal wells deeper than 3000 m, the addition of silica fume and industrial slag to the cement can effectively improve the high-temperature resistance of CBC and prevent the deterioration of the thermal conductivity.

Acknowledgements
This research was financially supported by National Natural Science Foundation of China (42162022), Guizhou Science and Technology Department Project (Qian Ke He Ping Tai Ren Cai [2021]5626; Qian Ke He Zhi Cheng [2020]4Y048).

Author contributions
YY: Writing-Original Draft, Writing-Review & Editing, Investigation. BL: Formal analysis, Visualization, Resources. LC: Conceptualization, Investigation. ML: Formal analysis, Supervision. YL: Methodology. HH: Project administration.

Availability of data and materials
All data used in this study are available by contacting the first author Y. Yang (ccteg_yang@163.com).

Declarations

Competing interests
The authors declare that they have no known competing financial interests or personal relationships that could have appeared to influence the work reported in this paper.

Received: 29 August 2023 Accepted: 10 January 2024
Published online: 28 January 2024

References
Abdul D, Wenqi J, Tanveer A. Prioritization of renewable energy source for electricity generation through AHP-VIKOR integrated methodology. Renew Energ. 2022;184:1018–32.
Alexander MG, Sergey AG. Nanoscale control of hydrated portland cement structure. Solid State Phenom. 2022;335:159–65.
Andaverde JA, Wong-Loya JA, Vargas-Tabares Y, Robles M. A practical method for determining the rheology of drilling fluid. J Petrol Sci Eng. 2019;180:150–8.
Asadi I, Shafigh P, Abu Hassan ZFB, Mahyuddin NB. Thermal conductivity of concrete—a review. J Build Eng. 2018;20:81–93.
Burger N, et al. Review of thermal conductivity in composites: mechanisms, parameters and theory. Prog Polym Sci. 2016;61:1–28.
Carvajal PE, Miketa A, Goussous N, Fulcheri P. Best practice in government use and development of long-term energy transition scenarios. Energies. 2022;15(6):2180.
Chalermphan N, Watcharapong W, Pailyn T, Arnon C. Compressive strength and thermal conductivity of water and air cured Portland cement-fly ash-silica fume mortars. Environ Eng Manag J. 2018;17(9):2023–30.
Chen Y, Li XY, Du HX. A review of high temperature properties of cement based composites: effects of nano materials. Mater Today Commun. 2023;35: 105954.
Dong S, Liu G, Zhan T, Yao Y, Ni L. A thermal conductivity prediction model of cement-based grouts for ground source heat pump. Int Commun Heat and Mass. 2022;135: 106079.
Espinosa-Paredes G, et al. Thermal property measurement of mexican geothermal cementing systems using an experimental technique based on the Jaeger method. Appl Therm Eng. 2002;22(3):279–94.
Estrada-Wiese D, Del Rio-Chanona EA, Del Rio JA. Stochastic optimization of broadband reflecting photonic structures. Sci Rep. 2018;8(1):1193.
Farzadian O, Yousefi F, Spitas C, Kostas KV. Phonon heat transport in two-dimensional phagraphene-graphene superlattice. Int J Heat Mass Tran. 2022;182: 121917.
Gong LL, Wang YH, Cheng XD, Zhang RF, Zhang HP. A novel effective medium theory for modelling the thermal conductivity of porous materials. Int J Heat Mass Tran. 2014;68:295–8.
Hamid A, Setiati R, Santoso A. Application foam agent to foam cement slurry for geothermal well drilling. J Phys: Conf Series. 2019;1402: 055011.
Honorio T, Bary B, Benboudjema F. Thermal properties of cement-based materials: multiscale estimations at early-age. Cement Concrete Comp. 2018;87:205–19.
Ivan O, Jan S. Hydration of tricalcium silicate at elevated temperatures. J Chem Technol Biot. 1973;23(9):661–7.
Jia GS, et al. Series-parallel resistance method based thermal conductivity model for rock-soil with low or high porosity. Geothermics. 2020;84: 101742.
Kadoya K, Matsunaga N, Nagashima A. Viscosity and thermal conductivity of dry air in the gaseous phase. J Phys Chem Ref Data. 1985;14(4):947–70.
Kamali M, Khalifeh M, Saasen A, Godoy R, Delabroy L. Alternative setting materials for primary cementing and zonal isolation—laboratory evaluation of rheological and mechanical properties. J Petrol Sci Eng. 2021;201: 108455.
Kang X, Ge L. Enhanced series-parallel model for estimating the time-dependent thermal conductivity of fly ash soil mixtures. Granul Matter. 2015;17(5):579–92.
Kong YN, Wang PM, Liu SH, Gao ZY. Hydration and microstructure of cement-based materials under microwave curing. Constr Build Mater. 2016;114:831–8.
Kurumisawa K, Nawa T, Owada H, Shibata M. Deteriorated hardened cement paste structure analyzed by XPS and 29Si NMR techniques. Cement Concrete Res. 2013;52:190–5.
Land G, Stephan D. Controlling cement hydration with nanoparticles. Cement Concrete Comp. 2015;57:64–7.
Lupyana SD, Maagi MT, Gu J. Common well cements and the mechanism of cement-formation bonding. Rev Chem Eng. 2022;38(1):17–34.
Macaulay BD, Bouazza A, Singh RM, Wang B, Ranjith PG. Thermal conductivity of soils and rocks from the Melbourne (Australia) region. Eng Geol. 2013;164:131–8.
Macenić M, Kurevija T, Medved I. Novel geothermal gradient map of the Croatian part of the Pannonian Basin System based on data interpretation from 154 deep exploration wells. Renew Sust Energ Rev. 2020;132: 110069.
Marazuela MA, Alejandro G-G. Frontier research of engineering: geothermal energy utilization and groundwater heat pump systems. Sustainability. 2022;14(21):13745.
Maxwell JC. A treatise on electricity and magnetism. Nature. 1873;7:478–80.

Molina-Rodea R, Wong-Loya JA. A new model to predict subsoil-thermal profiles based on seasonal rain conditions and soil properties. Geothermics. 2021;97: 102261.
Pang CW, Jung JY, Kang YT. Aggregation based model for heat conduction mechanism in nanofluids. Int J Heat Mass Tran. 2014;72:392–9.
Pelletier L, Winnefeld F, Lothenbach B. The ternary system Portland cement-calcium sulphoaluminate clinker-anhydrite: hydration mechanism and mortar properties. Cement Concrete Comp. 2010;32(7):497–507.
Powmrshelm JM, Clifton JR. Mathematical modeling of tricalcium silicate hydration. Cement Concrete Res. 1979;9(6):765–70.
Qomi MJA, Ulm FJ, Pellenq RJM. Physical origins of thermal properties of cement paste. Phys Rev Appl. 2015;3(6): 064010.
Rahman A, Farrok O, Haque MM. Environmental impact of renewable energy source based electrical power plants: solar, wind, hydroelectric, biomass, geothermal, tidal, ocean, and osmotic. Renew Sust Energ Rev. 2022;161: 112279.
Rajvikram ME, et al. A novel sustainable development goal 7 composite index as the paradigm for energy sustainability assessment: a case study from Europe. Appl Energy. 2022;307: 118173.
Razak HA, Sajedi F. The effect of heat treatment on the compressive strength of cement-slag mortars. Mater Design. 2011;32(8):4618–28.
Ren CZ, et al. Recycling of hazardous and industrial solid waste as raw materials for preparing novel high-temperature-resistant sulfoaluminate-magnesia aluminum spinel cement. J Build Eng. 2023;64: 105550.
Santoyo E, et al. Effective thermal conductivity of Mexican geothermal cementing systems in the temperature range from 28 ℃ to 200 ℃. Appl Therm Eng. 2001;21(17):1799–812.
Sełńczuk K, Sapińska ŚA, Kowalski T. Utilization of basalt dust as waste material in cement grouts for geothermal application. Energies. 2022;15(19):1–30.
Seungmin, L., 2015. Effects of elevated temperature exposure on cement-based composite materials. University of Illinois at Urbana-Champaign (Ph.D. Degree Dissertation).
Silvaa JC, Milestone NB. Cement/rock interaction in geothermal wells, the effect of silica addition to the cement and the impact of CO_2 enriched brine. Geothermics. 2018;73:16–31.
Tan KF, John MN. Performances of concrete under elevated curing temperature. J Wuhan Univ Technol Mater Sci Ed. 2004;19(3):65–7.
Tarnawski VR, Leong WH. A series-parallel model for estimating the thermal conductivity of unsaturated soils. Int J Thermophys. 2012;33(7):1191–218.
Tomasini-Montenegro C, Santoyo-Castelazo E, Gujba H, Romero RJ, Santoyo E. Life cycle assessment of geothermal power generation technologies: an updated review. Appl Therm Eng. 2017;114:1119–36.
Tosti L, Ferrara N, Basosi R, Parisi ML. Complete data inventory of a geothermal power plant for robust cradle-to-grave life cycle assessment results. Energies. 2020;13(11):2839.
Wang S, Jian LM, Shu ZH, Chen SH, Chen LY. A high thermal conductivity cement for geothermal exploitation application. Nat Resour Res. 2020;29(6):3675–87.
Won J, Lee D, Na K, Lee IM, Choi H. Physical properties of G-class cement for geothermal well cementing in South Korea. Renew Energ. 2015;80:123–31.
Wu, Y., Patel, H. and Salehi, S., 2020. Thermal considerations of cement integrity in geothermal wells. 45th Workshop on Geothermal Reservoir Engineering: SGP-TR-216 (Conference Article).
Xu JN. Drilling and completion techniques for high-temperature geothermal wells. Adv Mater Res. 2014;953–954:688–91.
Xu SL, Liu JH, Zeng Q. Towards better characterizing thermal conductivity of cement-based materials: the effects of interfacial thermal resistance and inclusion size. Mater Design. 2018;157:105–18.
Yang Y, et al. Investigation on the preparation, properties, and microstructure of high thermal conductive cementing material in 3500m-deep geothermal well. Geothermics. 2022;100: 102322.
Yu J, Choi HK, Kim HS, Kim SY. Synergistic effect of hybrid graphene nanoplatelet and multi-walled carbon nanotube fillers on the thermal conductivity of polymer composites and theoretical modeling of the synergistic effect. Compos Part A-Appl S. 2016;88:79–85.
Yuan RX, et al. Evaluation of shallow geothermal energy resources in the Beijing-Tianjin-Hebei Plain based on land use. J Groundw Sci Eng. 2021;9(2):129–39.
Zhang BB, et al. Effects of the bubbles in slag on slag flow and heat transfer in the membrane wall entrained-flow gasifier. Appl Therm Eng. 2017;112:1178–86.
Zhen ZW, De JS, De QJ. Study on the thermal conductivity model of cement-based materials by a new test method. Adv Mater Res. 2012;457–458:457–60.

Publisher's Note